




Electrochemical behaviour of lead-free Sn–0.7Cu–xIn solders alloys in 3.5 wt% NaCl solution

Dheeraj Jaiswal^{1,*} , Vikrant Singh¹, Dileep Pathote¹, and C. K. Behera¹

¹Department of Metallurgical Engineering, Indian Institute of Technology (BHU), Varanasi 221005, India

Received: 23 March 2021

Accepted: 12 August 2021

Published online:
21 August 2021

© The Author(s), under exclusive licence to Springer Science+Business Media, LLC, part of Springer Nature 2021

ABSTRACT

Various electronic equipment has been exposed to a very harsh atmospheric condition that results in corrosion of the solders inside it. The type of corrosion, in most cases, is electrochemical. The lead-free solders are mostly preferred as the solder. Electrochemical corrosion behaviour of lead-free solder Sn–0.7Cu alloys with a variation of indium of $x = 0–3$ wt% was studied in an air-saturated aqueous solution 3.5 wt% NaCl at room temperature. The potentiodynamic polarization test shows that corrosion resistance improves with In content. The addition of indium refines the microstructure and improve Sn–0.7Cu solder alloys' corrosion resistance by lowering the current density (I_{corr}), resulting in high resistance of the passive layer formed. XRD analysis shows that the composition of corrosion products also changed with indium content variation, phases such as $\text{Sn}_3\text{O}(\text{OH})_2\text{Cl}_2$, and oxides and chlorides of Sn were formed. Electrochemical impedance spectroscopy analysis shows that Indium addition changes the behaviour of the electrochemical interface from charge transfer to diffusion control.

1 Introduction

Soldering is one of the very important metallurgical method for joining various metal parts in electronic packaging and assemblies due to their excellent electrical interlinking property and mechanical support. Different electronic components are assembled with a lead-frame or directly (flip-chip technology) to a circuit board by this technique [1]. Soldering is a simple and effective procedure with several environmental and health disadvantages, which cannot be neglected. Because of the requirement of a lead-free alloy to solder, this research has become

essential. Among all other properties, the melting point is one of the most important ones. The ideal melting point of the material to qualify for as soldering alloy cannot be too high to generate any thermal issues or not be too low to become nonfunctional.

The electronic industry's prevailing choice has been a binary system of Sn–Pb solder alloys due to their low melting temperature. (m.p 183 °C), good wettability, and mechanical properties [1, 2]. The Eutectic alloy, e.g. 40Pb–60Sn, is the most widely used solder in industries. The replacement of lead alloy with a lead-free alloy of the same melting

Address correspondence to E-mail: dheerajjaiswal.rs.met17@itbhu.ac.in

temperature is complicated and has become a significant concern [3]. Given all of these benefits, toxicity of heavy metal like Pb has in recent times limited its use. According to the US Environmental Protection Agency [4], Pb and Pb containing compounds are hazardous chemicals in the top 17 list of chemicals and also a life threatening to humans and the environment [5, 6]. In the current scenario, the lead-free alloy for solder application can help in tackling the upcoming challenges related to the environment. To design a new solder alloy with the desired range of various characteristics like melting point, mechanical strength, microstructure, wettability, solderability, reliability, and cost must be investigated [7]. That electronic packaging method makes solders exposed directly to corrosion in air, moisture, and oceanic environments. Hence the reliability and life of electronic devices are impaired by the corrosion resistance of new solder alloys.

Researchers developed many binary lead-free solder alloys, including Sn–Zn, Sn–In, Sn–Bi, Sn–Sb, Sn–Ag, and Sn–Cu. It has also been predicted that the ternary metal alloy can provide an excellent opportunity to get a lead-free alloy.

Among tin-based lead-free solder alloys, Sn–Zn's family has advantages such as low reflowing temperature (198.5 °C) and high wettability among lead-free tin-based solder alloys. Since zinc is placed at a lower position in the electrochemical series, it is chemically active, which cause problems in the solder joint by forming zinc oxide/hydroxides. This makes solder is vulnerable to corrosion. The addition of silver could give the solder better corrosion resistance (Sn–9Zn–xAg). On the other hand, Sn–Bi eutectic solder alloy has a lower reflowing temperature (138 °C) than Pb–Sn solder alloys (183 °C). The handling of lead and its recovery has certain restrictions. It is found from the literature that after recycling, Pb emits a higher amount of α particle than pure lead, which causes a reduction in electronic circuit efficiency [8]. As an alternative to Pb–Sn solder alloys, the eutectic Sn–Cu alloy finds wide application due to lower cost. Although considered a good solder alternate to conventional solder, the effects on mechanical and corrosive resistance of various microstructural scales can be found in the literature, mainly concerned with adding a third element to the alloy [9]. A study on Sn–Cu solder alloys shows precipitation of Cu_6Sn_5 intermetallic phases in rod form in Sn matrix, which causes strain along the

grain boundaries resulting in a reduction in corrosion resistance. Eutectic reaction produces the Cu_6Sn_5 faceted intermetallic phases in rod form embedded in a continuous Sn rich matrix, causing strain between these phases along the grain boundaries. [9, 10]. The study has also shown that increasing copper content from 0.8 to 6.7 per cent leads to an increase in corrosion resistance [11]. The corrosion products formed on solder alloys samples exposed to NaCl media are challenging to understand with an aerated acidic NaCl solution. A complex layer of tin oxide, SnO_2 , $\text{Sn}_3\text{O}(\text{OH})_2\text{Cl}_2$ are observed in the corrosion product [12, 13].

The alloying process is an efficient way to obtain the refined microstructure of solders; Sn–0.7Cu alloy, for instance, it has been found that the refined microstructure was achieved after alloying with Ni, Ag, and Al, and there was an increase in the oxidation resistance [14, 15]. The addition of In will enhance the mechanical properties and wettability of Sn–0.7Cu [16].

Indium (In) is a valuable component for solving the high melting point and low wettability of solder alloy on Cu substrate [17, 18]. The main advantages of the addition of indium have a significant effect on the corrosion resistance of solder alloy Sn–0.7Cu. The addition of In the solder alloys of Sn–0.7Cu–xIn helps in improving corrosion resistance by forming a better passivation film during polarisation in 3.5 wt% NaCl protecting the surface against further corrosion [19–22]. Other researchers report many advantages to add indium in lead-free solder alloys. Decreases the melting temperature and increases the melting range, solder corrosion rate. It also improves the solder hardness, wettability of lead-free solder is improved [23]. Indium is responsible for lowering the thickness ratio of IMC $\text{Cu}_3\text{Sn}/\text{Cu}_6\text{Sn}_5$ is lowered, and Improved solder alloy corrosion resistance and shear strength [24, 25].

In this article, an attempt has been made to synthesize Cu–Sn–In alloys with different compositions of indium in this alloy, keeping the composition of the Cu and Sn constant by vacuum induction technique. Then the composition and morphology of the alloys were investigated by metallographic methods. Then the corrosion measurements were carried out to see the effect of indium on the corrosion resistance of the alloys by potentiodynamic polarization (PD) test and wet loss method. Subsequently, the samples were subjected to SEM and XRD analysis to analyze

the composition of the corrosion product. The corrosion mechanism was then predicted by combining the potentiodynamic polarization test and Electrochemical Impedance Spectroscopy (EIS).

2 Experimental procedure

2.1 Synthesis of Sn–0.7Cu–xIn solder alloys

Sn–0.7Cu–xIn ($x = 0, 1, 2, 3$ in wt%) ternary alloys were prepared by melting of pure Cu, In and Sn (purity > 99.9%). The constituents were weighed, kept in an alumina crucible (5 cm length and 2 cm diameter), and put in a vacuum induction furnace.

After that furnace was sealed and purged from the furnace chamber for 15 min with pure nitrogen gas for removed oxygen and other unwanted gas, the temperature of the furnace was increased by 4 °C/min up to 450 °C with 30 min of soaking time under the vacuum (10^{-4} torr). The molten alloys were then cooled down to 250 °C and subjected to furnace cooling, and further cooled for 24 h at room temperature. This alloy sample was again re-melted at the same temperature and vacuum conditions. The whole procedure of re-melting followed by furnace cooling and resting of alloy was repeated three times for the homogenization of metals. The solidified alloy sample was cleaned with acetone and subjected to a flat belt grinder to remove excess materials or imperfections present on the surface. The alloy sample was again polished using P 800 Electro coated silicon carbide waterproof paper from grade range 400–1200 and cloth polishing to smoothness the sample's surface. Scanning electron microscopy (SEM) was used to analyze corroded samples' microstructure and surface morphology, and compositional analysis was performed using energy dispersive spectrometry (EDS) and X-ray diffraction (XRD).

2.2 Potentiodynamic polarization and EIS tests

Lead-free solder alloys' working surface (10 mm dia.) was mechanically ground with SiC paper from 100 to 1600 grid mirrors polished with the help of 0.3 μm Al_2O_3 powder paste. The sample is ultrasonically cleaned in acetone and distilled water before

further characterization. Corrosion testing was conducted at room temperature in an air-saturated aqueous solution of 3.5 wt% NaCl solution prepared by dissolving 35 g of analytical grade Sodium chloride powder in deionized water from a 1-L solution.

The potentiodynamic polarization test was performed by the CorrTest Instruments Corp., Ltd. (Wuhan, China). The Potentiodynamic polarization scanning was performed in a 3.5 wt% NaCl solution with the laboratory atmosphere at room temperature (27 ± 5 °C).

This rectangular polarization cell had Pt wire as a counter electrode, Ag/AgCl as a KCl saturated reference electrode and an exposed solder alloys area (1 cm^2) that acted as an electrode practice. Before the Potentiodynamic polarization evaluation of Sn–0.7Cu–xIn solder alloys, open circuit potential (OCP) measurement was done for 30 min at 1Hz frequency to ensure that the specimen's working surface to be stable.

EIS then analyzes the resistance to corrosion at OCP over a frequency range from 0.01 Hz to 100 kHz. Potentiodynamic polarization analysis was taken after electrochemical impedance spectrograph (EIS) with potential range was scanned from -500 mV (vs. OCP) to 500 mV (vs. OCP) vs. $V_{\text{Ag}/\text{AgCl}}$ at 1 mV/s . The obtained data from potentiodynamic polarization and EIS tests were analyzed with CView (CS studio, version 5.2) and ZView (CS studio, version 5.2) software to obtain the corrosion rate and corrosion resistance, respectively (Fig. 1).

2.3 Characterizations

The specimen surface before the corrosion tests were observed using an optical microscope (OM, Leica Z6 APO) and also investigate their corroded and non-corroded surface microstructure morphology, a chemical composition by (SEM, ZEISS MA15/18, UK) equipped with energy dispersive spectroscopy (EDS) was used. Phase analysis was done using XRD (Rigaku MiniFlex, Japan) equipped with a hybrid pixel array detector with rotating Cu–K α . XRD analysis has taken scanning angle (2θ) from 20° to 90° with a scanning speed of $5^\circ/\text{min}$ with accelerating voltage of 40 KV and current 15 amperes. The XRD peak was analyzed by using X-part Highscore plus software to find different types of phases.

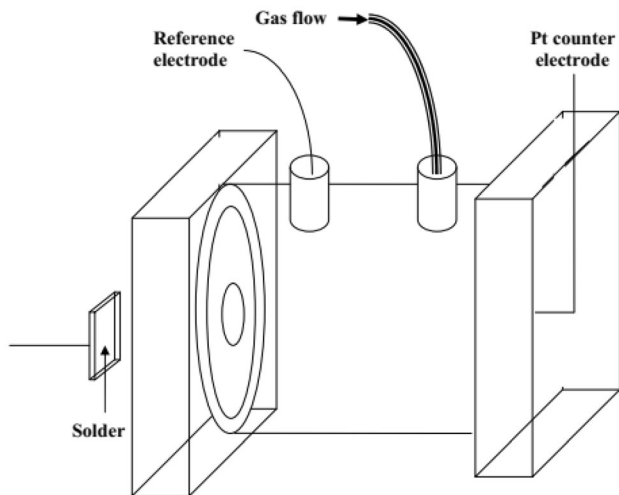


Fig. 1 Schematic diagram of a rectangular polarization cell

3 Results and discussion

3.1 Microstructure characterization

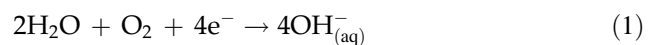
The SEM microstructure and EDS analysis of lead-free solder alloys Sn–0.7Cu–xIn ($x=0, 0.1, 0.2,$ and 0.3 wt%) are shown in Fig. 2. It showed two different contrast, one the dark region, which seems to be precipitation during solidification of Cu_6Sn_5 (IMC) and light phase of β -Sn phase matrix (2.d). Nucleation of binary Sn–0.7Cu liquid alloy takes place at approximately 227°C (eutectic temperature). Liquid Sn–0.7Cu transfers to β -Sn and Cu_6Sn_5 ($\text{L} \rightarrow \text{Cu}_6\text{Sn}_5/\text{Cu}_3\text{Sn} + \beta\text{-Sn}$), consistent with Sn–0.7Cu binary phase diagram. The main principal additives of the Sn–0.7Cu solidified alloys are Cu_6Sn_5 and β -Sn. At eutectic temperature (227°C), the dissolution of the Cu_6Sn_5 is triggered, and the Cu_6Sn_5 eutectic is grown through β -Sn diffusion. A small volume of Cu_2In phase precipitated seen in Sn–0.7Cu–xIn solder alloy due to indium's addition from 1 to 3 wt% in the Sn–0.7Cu solder alloy. The uniform microstructure of Sn–Cu–In solder alloys has been obtained with the addition of the Indium element, and β -Sn grains have significantly been refined. The microstructure of refined solder alloys contributed to a more uniform phase distribution, which benefited the superior mechanical properties [26].

The experiment was carried out with XRD, and corresponding results are shown in Fig. 3. One can see that Sn–0.7Cu, Sn–0.7Cu–1In, Sn–0.7Cu–2In, and Sn–0.7Cu–3In consist of the pattern of β -Sn, Sn_3Cu , Sn_6Cu_5 , and Cu_2In , while a pattern of variation of

Indium in Sn–0.7Cu includes some Cu_2In peaks with 2 theta scale between 43° and 45° .

3.2 Potentiodynamic polarization behavior

Sn–0.7Cu–xIn solder alloys potential current density curve produced by Potential polarization studies done in 3.5 wt% aerated NaCl solution in Fig. 4. Apparently, and all the alloys studied exhibit the same polarisation behaviour for variation of Indium from 0 to 3 wt% in Sn–0.7Cu–xIn solder alloys. The region of AB in the curve shows the cathodic reaction. During the potentiodynamic polarization experiment, the solution is directly reacted with the laboratory atmosphere, the initial reduction of oxygen in the neutral and aqueous solution.



The cathodic reaction was responding to metallic corrosion. It is carried by the oxygen reaction and/or hydrogen reaction. The hydrogen bubble produces at the working (cathode) electrode by reduction of water molecules and removal of hydrogen ions, which many researchers have reported [27–29].



An anodic reaction in the potentiodynamic polarization tests also occurs in particular regions, named BC, CD, DE and EF, as shown in a curve.

In the anodic region, current increases with increasing voltage (BC), which shows corrosion product formation. It has been demonstrated that the initial period formation of $\text{Sn}(\text{OH})_2$ takes place by reaction 4. After the appearance of the corrosion product. It covers the whole surface, which restricts current flow by increasing the resistance. As the thickness of the oxide layer, it results in no change of current density. Also, from Fig. 4 CD region plateau area, there is no change in current density and is stable at a value of about -4 A/cm^2 . This behaviour is called the passivation of an oxide layer. The current density increases dramatically from point B to point C, and corrosion product formation during the experiment has been tracked. It's far typically interpreted that the passivation film formation starts with the precipitation of $\text{Sn}(\text{OH})_2$ at the surface. Such corrosion products cover the alloys' surface and

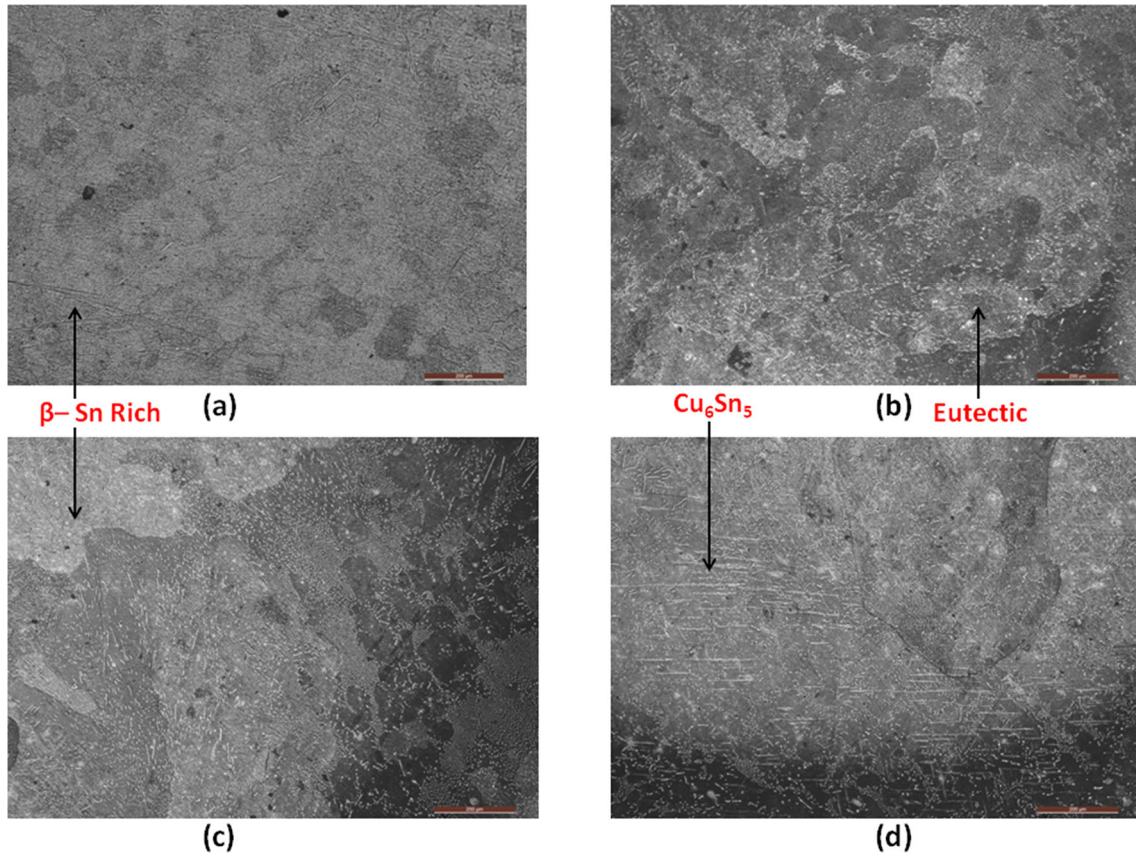


Fig. 2 Optical microstructures solder alloys a Sn-0.7Cu, b Sn-0.7Cu-1In, c Sn-0.7Cu-2In, and d Sn-0.7Cu-3In

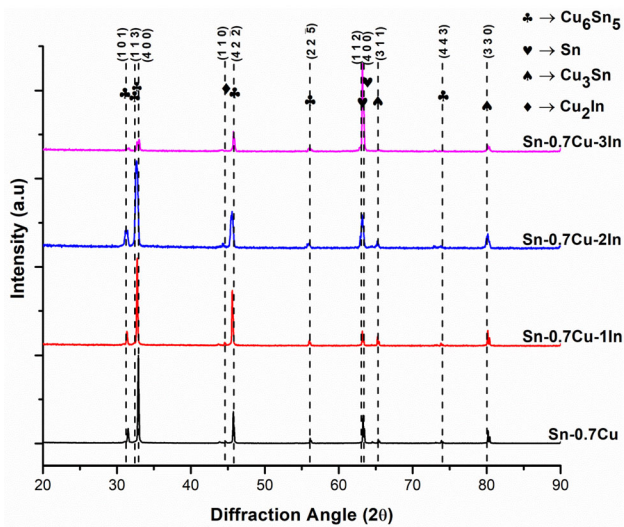


Fig. 3 XRD pattern of Sn-0.7Cu-xIn solder alloys

protect the substratum alloys against further corrosion; thus, a plateau area (CD) occurs in curves where the current density maintains a relatively stable value of about -4 A/cm^2 . This stage illustrates the

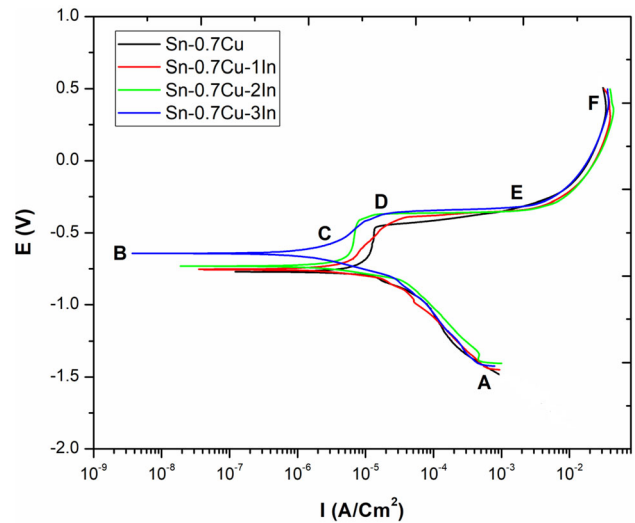
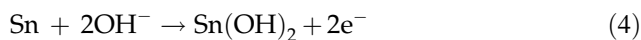


Fig. 4 Potentiodynamic polarization curves of Sn-0.7Cu-xIn solder alloys in 3.5 wt% NaCl solution

passivation behaviour and subsequent successful dissolution of Sn, as shown in Equation 4.



A sharp increase in current density is again located when the potential reaches point D, signalling the passivation film's breakdown, usually due to the oxygen evolution reaction in Eq. 4 and the absorption of Cl^- by corrosion products. Tin monoxide (SnO) has been considered as semiconductor oxide and may weaken the corrosion resistance. Hence it is detrimental to the passivation film's stability. These results in a sharp peak corresponding to active Sn dissolution induced by Cl^- ions with the formation of SnCl_3^- and SnCl_6^{2-} soluble complexes, resulting in the initial pitting, which inevitably breaks the passivation layer consistency. The tin oxide was formed found to be thermodynamically stable. Therefore so tin hydroxides can quickly dehydrate to form SnO_2 and SnO .

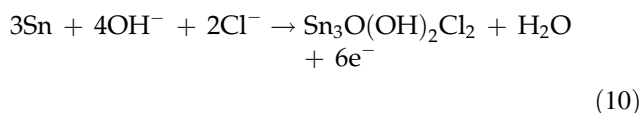
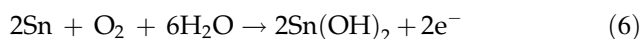


Table 1 summarizes the relevant Tafel fitting findings of the polarization test. Due to the lack of a well-defined investigation anodic, the corrosion current density (I_{corr}) was determined by extrapolating the cathodic Tafel area. The corrosion potential (E_{corr}) favourably shifted to a more negative value from -770.16 to -731.27 mV, increasing the weight percentage of indium from 1 to 3 wt%. The potential corrosion increases with the increases in the indium content of the alloys. A nobler E_{corr} value means that the alloys are thermodynamically resistant to corrosion. Therefore, it is simple to find that adding one weight percentage of In will effectively increase the

alloy's corrosion resistance from the thermodynamic aspect. It is also observed that corrosion current density (I_{corr}) value for Sn–0.7Cu solder alloy decreases significantly with the addition of In, especially for Sn–0.7Cu–3In alloys. In general, I_{corr} is a crucial parameter for evaluating the corrosion rate and the kinetics of corrosion reactions at E_{corr} .

As shown in Table 1, the adding of Indium in Sn–0.7Cu alloy decreases I_{corr} value and an improved protective layer of a passivation film on the surface of a sample by the inclusion of indium. This result may be attributed to the Indium involvement in passivation behaviour, as submitted by Tao-Chil Chang et al. It could be concluded that the additional small quantity of Indium in Sn–0.7Cu alloys may increase the corrosion resistance. The addition of more indium could possible give the better corrosion resistance of the above alloys.

3.3 EIS analysis

EIS has been used to analyze the corrosion resistance of lead-free solder alloys at OCP. Nyquist plots (complex impedance) and Bode plots for Sn–0.7Cu– x In ($x = 0, 1, 2, 3$) are illustrated in Fig. 5a and b. Impedance plots are shown for the different compositions with the variation of indium in solder alloys. It is seen that the Nyquist plots consist of a single depressed semicircle, while the Bode plots indicate a constant presence within the impedance spectra. Current distribution patterns were calculated using EIS. If phase angles are greater than 45° in the phase angle vs. $\log f$ plots, the current distribution is uniform in the given frequency region. Therefore an effective corrosion rate can be measured from the potential polarization curve. All indium containing Sn–0.7Cu alloys have a straight line at the low-frequency region, whereas Sn–0.7Cu alloy has a semi-circular arc when superimposing with two axes angle of about 45° . It shows that the corrosion kinetics process shifts from charge transfer control in Sn–0.7Cu alloy to diffusion control in indium based

Table 1 Polarization parameters for Sn–0.7Cu– x In alloys in 0.5 M NaCl solution

Sample	I_{corr} (μ Amps/cm ²)	E_{corr} (mVolts)	Corrosion rate (mm/y)* 10^{-2}
Sn–0.7Cu	24.828	– 770.16	8.113
Sn–0.7Cu–1In	12.034	– 731.27	3.9326
Sn–0.7Cu–2In	4.691	– 722.97	1.533
Sn–0.7Cu–3In	2.468	– 642.85	0.80654

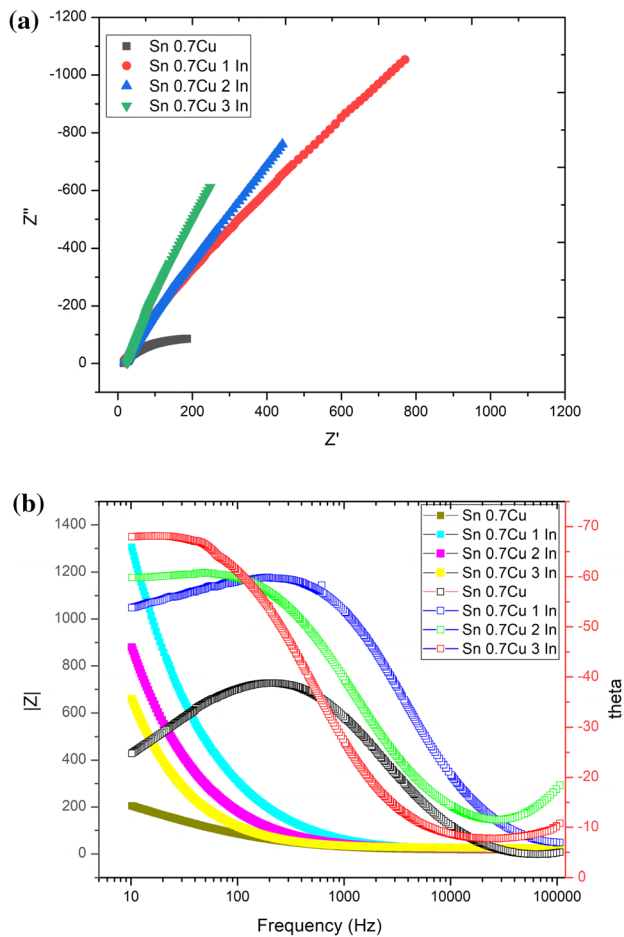


Fig. 5 **a** Nyquist and **b** Bode plots of solder alloys in 0.5 M NaCl solution

alloys known as Warburg impedance. Its means addition of Indium in Sn–0.7Cu alloys changes the corrosion mechanism of alloys. Bode plots are shown in Fig. 4b; most phase angle curves are lower than 90°, which means an ideal capacitance deviation concerning the electrochemical interface is present. In the high-frequency region, the arc radius for Sn–0.7Cu–3In is high compared to the lower composition of indium alloys, which means that Sn–0.7Cu–3In has been the best corrosion-resistant alloy in this study. Two other equivalent electrical circuits (EEC) models are used to fit EIS data to Sn–0.7Cu and Indium containing Sn–0.7Cu alloys based on the above interpretation.

Figure 6 shows, A simple equivalent circuit (EC) is reliable to be a Randle cell circuit R_s is the resistance o the solution, CPE_1 and R_1 were related to the capacitance and resistance of the porous product layer of corrosion; CPE_2 and R_2 were related to the

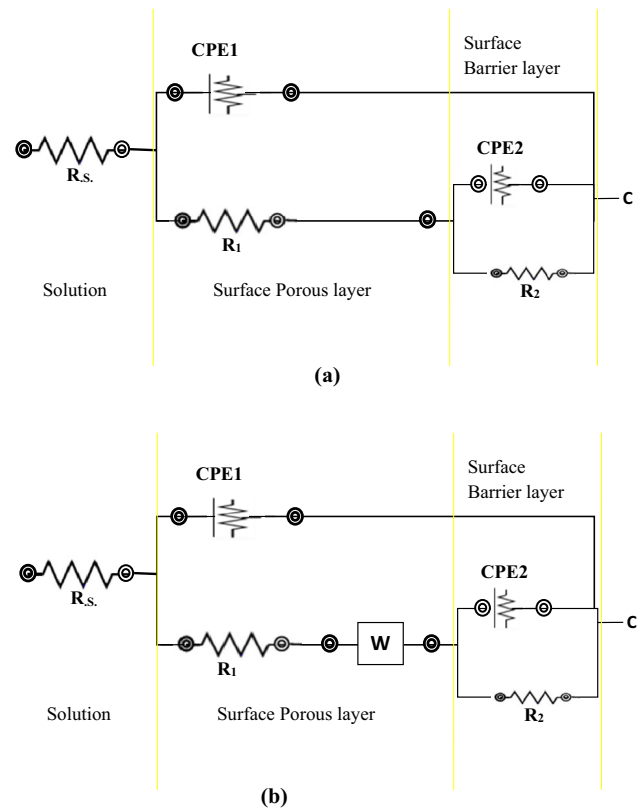


Fig. 6 Electrical circuit models. **a** For Sn–0.7Cu alloy; **b** For Sn–0.7Cu alloys with Indium addition

capacitance and resistance of the electrical double layer between the alloys interface and the product of corrosion and W related to the Warburg impedance respectively.

The fitting parameter comes out from EIS data ware well-fitting in EEC modal is summarized in Table 2. The results obtained after fitting are evaluated with a standard deviation (χ^2) at a magnitude of about 10^{-4} . So we may assume that the proposed EEC models are adequate for quantitative evaluation of the electrochemical interface’s behaviour.

It should be noted that almost all of the alloys in this experiment contain the same resistance solution (R_s) using the same concentration solution in this experiment. The R_1 value of such indium based alloys is often higher than that of the Sn–0.7Cu alloy R_1 reflects corrosion resistance of a porous surface layer of corrosion, as described above, and it can be concluded that the introduction of indium will lead to a more protective surface layer of corrosion. To quantitatively evaluate the total corrosion resistance to corrosion of the solder alloys introduce by $R_t = -R_w + R_1 + R_2$ [30, 31]. Throughout this study, the

Table 2 Fitting parameters of EEC for Sn–0.7Cu–xIn alloys in 0.5 M NaCl solution

Sample	$R_s \Omega \text{ cm}^2$	$R_1 \Omega \text{ cm}^2$	CPE ₁		$R_2 \Omega \text{ cm}^2$	CPE ₂		$R_w \Omega \text{ cm}^2$	$\chi^2 * 10^{-4}$
			$Y_1 * 10^{-6} \Omega \text{ cm}^{-2} \text{ s}^n$	n_1		$Y_2 * 10^{-6} \Omega \text{ cm}^{-2} \text{ s}^n$	n_2		
Sn–0.7Cu	14.54	21.19	127.86	0.6912	202.5	178.71	0.61056		0.15477
Sn–0.7Cu–1In	18.7	7.556	26.92	0.7519	1807	29.849	0.7160	3100	0.1611
Sn–0.7Cu–2In	17.14	21.55	450.59	0.4962	5476	45.482	0.7523	4666	1.8286
Sn–0.7Cu–3In	19.1	25.75	376.02	0.5677	22,393	51.733	0.5677	1.49	1.3499

total resistance of alloys extended due to the Warburg impedance in this experiment; solution resistance R_s is not considered because it is almost constant due to the same solution. Therefore total Resistance of Sn–0.7Cu–xIn ($x = 0, 1, 2, 3$) is 0.2236, 4.9145, 10.1635 and 22.4202 respectively. It is seen that R_1 increases with the increase in Indium content Indium in alloys. Therefore then Sn–0.7Cu–3In has the highest Rt value. It can be inferred from the observation that the indium addition in the Sn–0.7Cu alloy will improve the corrosion resistance in this experiment.

3.4 Characterization of corrosion products

Surface topography of solder alloys was done by SEM and composition analysis by EDS and XRD. IT was done before and after the electrochemical corrosion in 0.5M NaCl. Generally, the morphology of alloys' surface changes forms smooth to porous due to the formation of branched crystallites, networked branches, platelet-like and sponge-like structures. EDS and XRD analysis have recognized such compounds as mainly tin oxide and other corrosion products. The addition of indium from 1 to 3 wt% in binary Sn–0.7Cu solders in Fig. 7 shows that all the solder alloys surface after corrosion was covered by a sponge platelet-like structure of different sizes. It has been observed that sponge-like structures are denser in the Sn–0.7Cu–3In sample than the Sn–0.7Cu solder alloys. There is not much difference in quantity and morphology of corrosion product Sn–0.7Cu and Sn–0.7Cu–1In. It is expected that the properties of corrosion products on the surface alloys should be denser, more refined, and continuous. Because it improves corrosion resistance by effectively protecting corrosion of alloys, it is evident from the EIS results that RP values for the porous product layer are higher, which is very valid for the denser porous

product layer. Therefore, the denser product layer on the solder alloys is very much helpful for the better corrosion resistance of the Sn–Cu–In alloys.

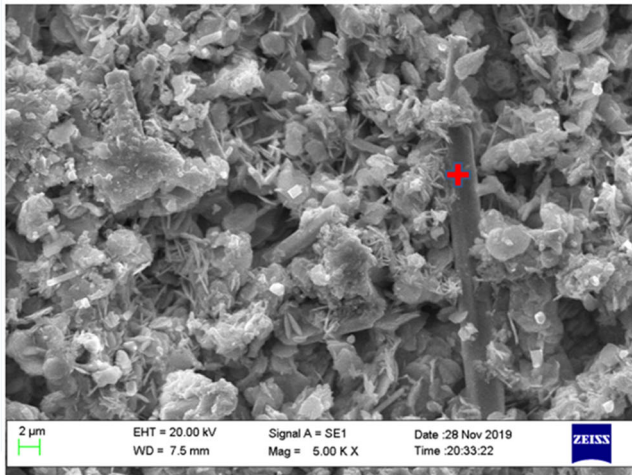
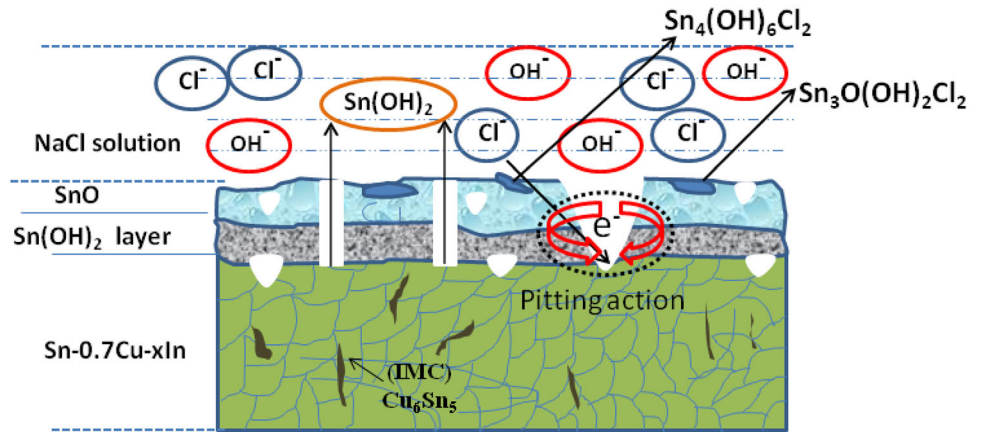
The EDX analysis of corrosion products of alloys is shown in Fig. 8 for all alloys taken for these investigations. There is a quite significant quantity of O, Na, Cl, Cu, and Sn present on the surface of the alloys after corrosion, while the Indium weight percentage is significantly less. The atomic percentage of Sn, H, Cl, and O in the corrosion products is more likely to consist of $\text{Sn}_3\text{O}(\text{OH})_2\text{Cl}_2$ on alloys' surface as a dominant product, mostly combined with small quantities of oxide compounds.

The XRD analysis was further carried out to confirm the phase composition of the corrosion products. Chloride can be explained by the presence of by-products of corrosion like chloride can be explained by the presence of by-products of corrosion like $\text{Sn}_3\text{O}(\text{OH})_2\text{Cl}_2$ [32] and $\text{Sn}_4(\text{OH})_6\text{Cl}_2$ [33] on the surface of alloys, and shown in Fig. 9.

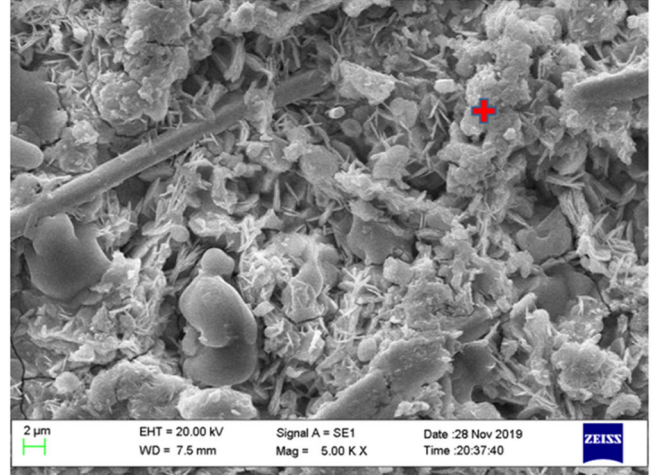
First, during the corrosion process, the surface layer decomposition and then pitting corrosion generally take place [34, 35]. Different kinds of models have been suggested to explain the corrosion mechanism in which aggressive anions such as OH^- and Cl^- play a significant role. It has been observed that faceted IMC of $\text{Cu}_6\text{Sn}_5/\text{Cu}_3\text{Sn}$ and non-faceted $\beta\text{-Sn}$ phase [36] are present in these lead-free solder alloys. $\text{Cu}_6\text{Sn}_5/\text{Cu}_3\text{Sn}$ particles are electrochemically nobler than tin. Therefore, a galvanic cell may be formed between the Sn-rich phase and IMC $\text{Cu}_6\text{Sn}_5/\text{Cu}_3\text{Sn}$, accelerating Sn–0.7Cu–xIn alloy's anodic corrosion.

Furthermore, the microstructural arrangement sets different cathode/anode area ratios. This is closely linked to the morphology and uniform distribution, as well as to the network interconnectivity level in the (noble) stage of the cathode (dendritic) cellular arrays [37]. For example, an integrated, interconnected network of IMC Cu_6Sn_5 formed in Sn–0.7Cu solder alloy

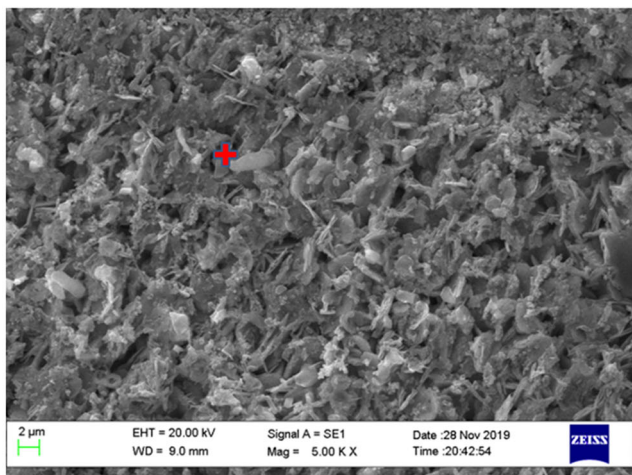
Fig. 7 Corrosion mechanism of solder alloys



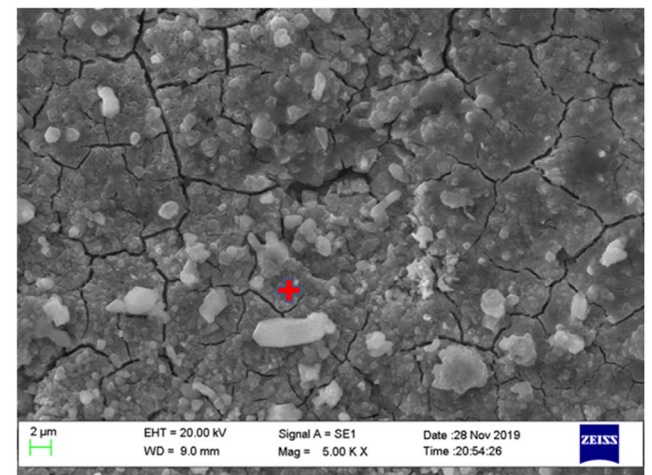
(a)



(b)



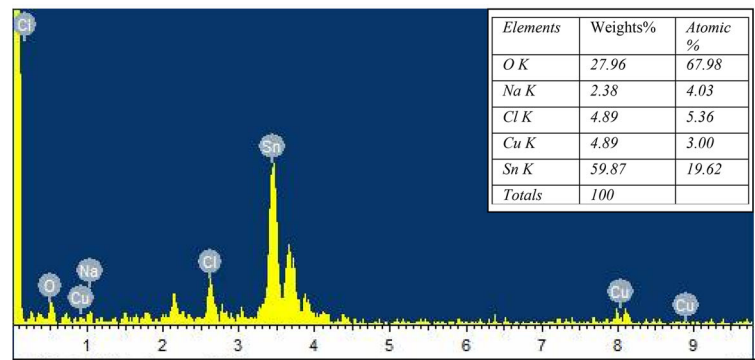
(c)



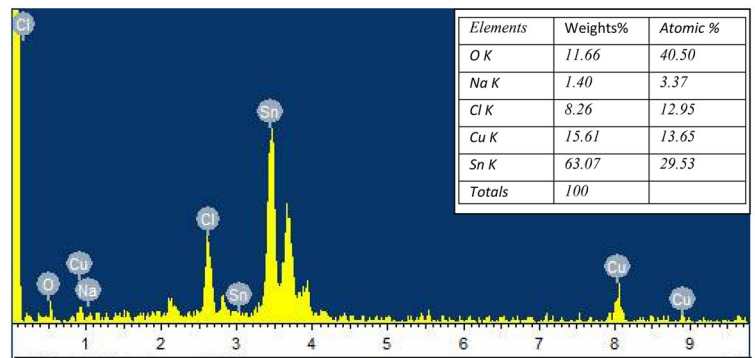
(d)

Fig. 8 Surface morphology of alloys after corrosion in 3.5 wt% NaCl. a Sn-0.7Cu; b Sn-0.7Cu-1In; c Sn-0.7Cu-2In; d Sn-0.7Cu-3In

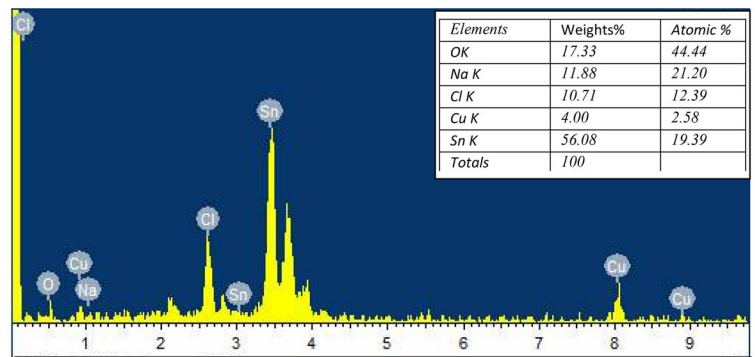
Fig. 9 EDX patterns of corrosion products. **a** Sn–0.7Cu; **b** Sn–0.7Cu–In; **c** Sn–0.7Cu–2In; **d** Sn–0.7Cu–3In



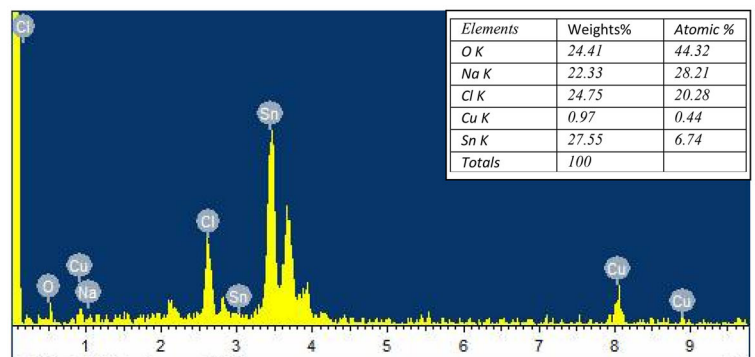
(a)



(b)



(c)



(d)

Fig. 10 XRD patterns of corrosion products. **a** Sn–0.7Cu; **b** Sn–0.7Cu–1In; **c** Sn–0.7Cu–2In; **d** Sn–0.7Cu–3In

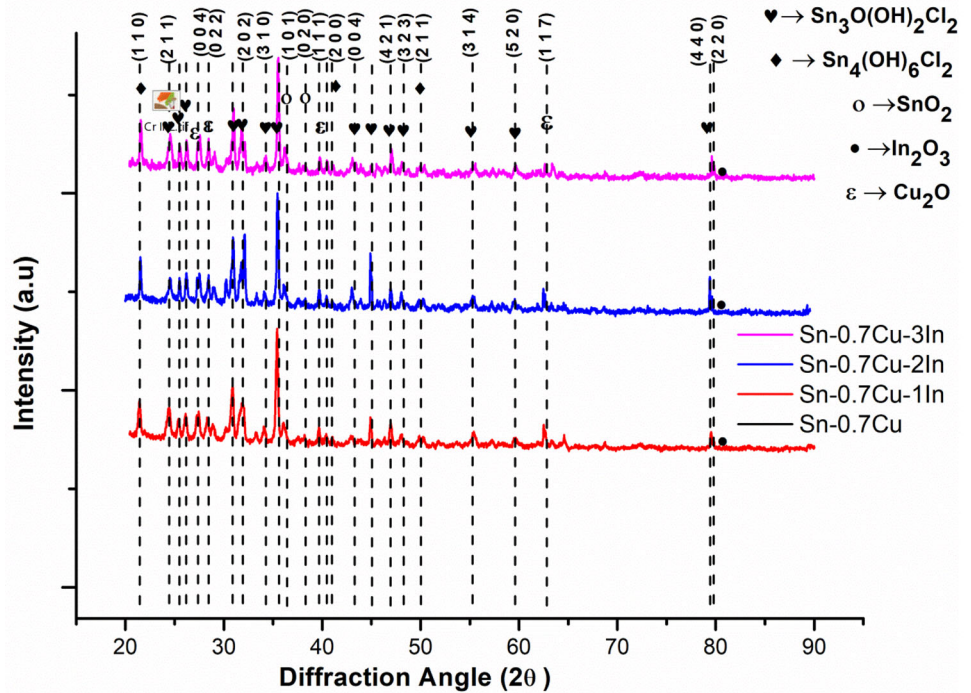


Table 3 Crystallite size of lead-free Sn–0.7Cu–xIn solder alloys

S. No.	Sample	Crystallite size [Å]				
		Sn ₃ O(OH) ₂ Cl ₂	Sn ₄ (OH) ₆ Cl ₂	SnO ₂	Cu ₂ O	In ₂ O ₃
1	Sn–0.7Cu	390	203	74	133	
2	Sn–0.7Cu–1In	473	258	98	184	62
3	Sn–0.7Cu–2In	503	309	121	203	69
4	Sn–0.7Cu–3In	532	349	135	231	76

[38] changes the cathode-anode ratio significantly with corrosion action. This increases the cathode area formed by Cu₆Sn₅ IMC, whereas the Sn-rich matrix is corroded intensely and more rapidly. The IMC of Cu₆Sn₅/Cu₃Sn thickness ratio decreases due to the addition of Indium particle in binary Sn–0.7Cu solder alloy, improving corrosion resistance [39].

The cathodic reaction results in the formation of OH[−] ions. Sn dissolution starts with an anodic reaction which results in the formation of Sn(OH)₂. Generally, Snⁿ⁺ has a valance state of *n* = 2 and *n* = 4, and it undergoes in scale form of Sn²⁺ or Sn⁴⁺ by giving e^{2−} or e^{4−}. The diffusion of Sn²⁺ atoms along the grain boundary results in the formation of a vacancy in the fat matrix. The reaction between these ions results in the formation of uniform Sn(OH)₂ and Sn(OH)₄ films, and the dehydration reaction of Sn(OH)₂ leads to the formation of SnO at the surface. The diffusion of Sn from the SnO layer at the surface

results in the formation of vacancies in the oxide layer. The dissolution of the oxide layer starts with the transfer of Sn ions from the SnO layer to the electrolyte, which results in the formation of Sn(OH)₂ in the electrolyte. This results in localized thinning of the film. The diffusion of Sn ions from the oxide layer causes the generation of vacancies in SnO film more quickly at the scale matrix interface, resulting in a breakdown of the passive SnO layer. Cl[−] anion attacks on the Sn matrix result in pits forming at the surface, as shown in Fig. 7 and 10.

Corrosion by-products for 3% In in Sn–0.7Cu–xIn contains highest Cl[−] atomic % (20.28%) compared to non doped In in its solder (atomic % of Cl[−] is 5.36%). It could be due to the porous nature of the oxide layer, which is formed at the surface which can absorb Cl[−]—while in the case of non-doped solder alloy, the oxide layer is broken, which leads to higher Cl[−]—concentration at the oxide metal interface, not at

Table 4 Lattice strain of lead-free Sn–0.7Cu–xIn solder alloys

S. No.	Sample	Lattice strain [%]				
		Sn ₃ O(OH) ₂ Cl ₂	Sn ₄ (OH) ₆ Cl ₂	SnO ₂	Cu ₂ O	In ₂ O ₃
1	Sn–0.7Cu	0.38	0.802	1.279	1.121	
2	Sn–0.7Cu–1In	0.29	0.433	0.981	0.931	1.242
3	Sn–0.7Cu–2In	0.043	0.517	0.598	0.783	1.231
4	Sn–0.7Cu–3In	0.051	0.223	0.562	0.551	1.084

the oxide surface. Since EDS analysis was done at the surface of the oxide layer, the concentration difference was observed. Similar behaviour was also observed by “Paper reference” [40, 41].

The crystallite size can be calculated on the corrected diffraction profile using full width at half maximum intensity (FWHM).

$$\text{Crystalline size} = \frac{K\lambda}{\beta_{\text{Sample}} \cos \phi}$$

K = Scherrer constant, λ = Wave length of radiation, β = width of the diffraction peak.

The full-width angle indicates the above width of the diffraction point at half the peaks of the XRD pattern.

This study found that the average crystallite size of all corrosion products increases with increasing indium in binary lead-free Sn–0.7Cu solder alloys and decrease lattice strain [42].

Thus, increasing the indium content leads to the microstructure parameters being increased (average crystal size) [43] (Tables 3 and 4).

4 Conclusions

The electrochemical behaviour of Sn–0.7Cu–xIn lead-free solder alloys in a natural 3.5 wt% NaCl was studied by potentiodynamic polarization tests and EIS measurements. The impact of Indium content on corrosion properties of Sn–0.7Cu–xIn solder alloys was investigated, and the following conclusions were drawn from these studies.

1. An increase of indium content from 1 to 3 weight percentage leads to a significant improvement in corrosion resistance of Sn–0.7Cu solder alloys, resulting in a higher range of pseudo passivation and lower current density pseudo passivation.
2. The addition of Indium to Sn–Cu binary solder alloys β -Sn grains have significantly. The resulting microstructure of fine solder alloys has now a more uniform distribution of various phases,

which is responsible for improving corrosion resistance.

3. The addition of Indium in Sn–0.7Cu solder alloys modifies the morphology of corrosion products on alloys' surface and change the corrosion kinetics from the charge transfer to the diffusion control process.
4. The corrosion products on the surface of all solder alloys studied after potentiodynamic polarisation consists of tin oxide chloride hydroxide Sn₃O(OH)₂Cl₂ and Sn₄(OH)₆Cl₂. Most corrosion products have plate-like shapes and were loosely distributed on the surface with different orientations.
5. Increase the indium content lead to increase crystallite size and decrease lattice strain.

References

1. H. Ma, J. Suhling, A review of mechanical properties of lead-free solders for electronic packaging. *J. Mater. Sci.* **44**, 1141–1158 (2009)
2. L.C. Tsao, Corrosion Resistance of Pb-Free and Novel Nano-Composite Solders in Electronic Packaging. (2006)
3. K.N. Tu, K. Zeng, Tin-lead (SnPb) solder reaction in flip chip technology. *Mater. Sci. Eng. R Rep.* **34**(1), 1–58 (2001)
4. N. Barry, University of Birmingham Research Archive. (2008)
5. E.P. Wood, K.L. Nimmo, C.T. Centre, S. Lane, U. Kingdom, *J. Electron. Mater.* **23**(8), 709 (1994)
6. P. Mishra, S.N. Alam, R. Kumar, Effect of Rare Earth Elements on Lead Free Solder Alloys. (2014); 80–86
7. Y. Kim, K. Kim, C. Hwang, K. Sukanuma, Effect of composition and cooling rate on microstructure and tensile properties of Sn–Zn–Bi alloys. *J. Alloys Compd.* **352**, 237–245 (2003)
8. C. Zweben, Metal-matrix composites for electronic packaging. *JOM [Internet]* **44**(7), 15–23 (1992). <https://doi.org/10.1007/BF03222270>

9. F. Song, S.W.R. Lee, C.W. Bay, H. Kong, Investigation of the effect of PCB base materials and pad surface finish on the thermal fatigue life of lead-free solder joints of PBGA and passive resistors, in *International Conference on Electronic Materials and Packaging*. (IEEE, Hong Kong, 2006)
10. K. Nogita, Intermetallics stabilisation of Cu_6Sn_5 by Ni in Sn–0.7Cu–0.05Ni lead-free solder alloys. *Intermetallics* [Internet]. **18**(1), 145–149 (2010). <https://doi.org/10.1016/j.intermet.2009.07.005>
11. F. Rosalbino, E. Angelini, G. Zanicchi, R. Marazza, Corrosion behaviour assessment of lead-free Sn–Ag–M (M = In, Bi, Cu) solder alloys. *Mater. Chem. Phys.* **109**(2–3), 386–391 (2008)
12. L.C. Tsao, C.W. Chen, Corrosion characterization of Cu–Sn intermetallics in 3.5 wt.% NaCl solution. *Corros. Sci.* [Internet]. **63**, 393–398 (2012). <https://doi.org/10.1016/j.corsci.2012.06.015>
13. Y.F. Gao, C.Q. Cheng, J. Zhao, L.H. Wang, X.G. Li, Electrochemical corrosion of Sn–0.75Cu solder joints in NaCl solution. *Trans. Nonferrous Met. Soc. China (English Ed)* [Internet]. **22**(4), 977–982 (2012). [https://doi.org/10.1016/S1003-6326\(11\)61273-9](https://doi.org/10.1016/S1003-6326(11)61273-9)
14. L. Yang, Y. Zhang, J. Dai, Y. Jing, J. Ge, N. Zhang, Microstructure, interfacial IMC and mechanical properties of Sn–0.7Cu–xAl ($x=0-0.075$) lead-free solder alloy. *Mater. Des.* [Internet]. **67**, 209–216 (2015). <https://doi.org/10.1016/j.matdes.2014.11.036>
15. X. Hu, Y. Lai, X. Jiang, Y. Li, Effects of In addition on the wettability, interfacial characterization and properties of ternary Sn–Cu–Ni solders. *J. Mater. Sci. Mater. Electron.* [Internet]. **29**(21), 18840–18851 (2018). <https://doi.org/10.1007/s10854-018-0009-x>
16. A.E. Hammad, Enhancement of creep resistance and thermal behavior of eutectic Sn–Cu lead-free solder alloy by Ag and In-additions. *Mater. Des.* [Internet]. **40**, 292–298 (2012). <https://doi.org/10.1016/j.matdes.2012.04.007>
17. M.S. Yeh, Effects of Indium on the mechanical properties of ternary Sn–In–Ag solders. *Metall. Mater. Trans.* **34**, 361–365 (2003)
18. S. Yu, C. Liao, M. Hon, M. Wang, The effects of flux on the wetting characteristics of near-eutectic Sn–Zn–In solder on Cu substrate. *J. Mater. Sci.* **5**(2), 4217–4224 (2000)
19. L. Yang, Y. Zhang, C. Du, J. Dai, N. Zhang, Effect of aluminum concentration on the microstructure and mechanical properties of Sn–Cu–Al solder alloy. *Microelectron. Reliab.* [Internet]. **55**(3–4), 596–601 (2015). <https://doi.org/10.1016/j.microrel.2014.12.017>
20. M.F. Mohd Nazeri, A.A. Mohamad, Corrosion resistance of ternary Sn–9Zn–xIn solder joint in alkaline solution. *J. Alloys Compd.* [Internet]. **661**, 516–525 (2016). <https://doi.org/10.1016/j.jallcom.2015.11.184>
21. T.-C. Chang, J.-W. Wang, M.-C. Wang, M.-H. Hon, Solderability of Sn–9Zn–0.5Ag–1In lead-free solder on Cu substrate. *J. Alloys Compd.* **422**(1–2), 239–243 (2006)
22. A. Jouaiti, M. Boulghallat, A. Zrineh, R. Lbibb, A. Sabbar, H. Oulfajrite, Electrochemical behavior of a new solder material (Sn–In–Ag). *Mater. Lett.* **57**(28), 4368–4371 (2003)
23. L.F. Li, Y.K. Cheng, G.L. Xu, E.Z. Wang, Z.H. Zhang, H. Wang, Effects of indium addition on properties and wettability of Sn–0.7Cu–0.2Ni lead-free solders. *Mater. Design* **64**, 15–20 (2014)
24. H. Fallahi, M.S. Nurulakmal, A.F. Arezodar, J. Abdullah, Effect of iron and indium on IMC formation and mechanical properties of lead-free solder. *Mater. Sci. Eng. A* [Internet]. **553**, 22–31 (2012)
25. A.A. El-daly, F. El-tantawy, A.E. Hammad, M.S. Gaafar, E.H. El-mossalamy, A.A. Al-ghamdi, Structural and elastic properties of eutectic Sn–Cu lead-free solder alloy containing small amount of Ag and In. *J. Alloys Compd.* [Internet]. **509**(26), 7238–7246 (2011). <https://doi.org/10.1016/j.jallcom.2011.01.062>
26. T.I. Zubar, V.M. Fedosyuk, A.V. Trukhanov, N.N. Kovaleva, K.A. Astapovich, D.A. Vinnik et al., Control of growth mechanism of electrodeposited nanocrystalline NiFe films. *J. Electrochem. Soc.* [Internet]. **166**(6), D173–D180 (2019). <https://doi.org/10.1149/2.1001904jes>
27. S.C. Chung, J.R. Cheng, S.D. Chiou, H.C. Shih, EIS behavior of anodized zinc in chloride environments. *Corros. Sci.* **42**, 1249–1268 (2000)
28. M. Mouanga, P. Berçot, Comparison of corrosion behaviour of zinc in NaCl and in NaOH solutions; Part II: electrochemical analyses. *Corros. Sci.* [Internet]. **52**(12), 3993–4000 (2010). <https://doi.org/10.1016/j.corsci.2010.08.018>
29. Q. Li, X. Liu, S. Lu, Corrosion behavior assessment of tin-lead and lead free solders exposed to fire smoke generated by burning polyvinyl chloride. *Mater. Chem. Phys.* [Internet]. **212**, 298–307 (2018). <https://doi.org/10.1016/j.matchemphys.2018.03.057>
30. F.E. Heakal, A.M. Fekry, A.A. Ghoneim, Corrosion characterization of new tin–silver binary alloys in nitric acid solutions. *Corros. Sci.* **50**, 1618–1626 (2008)
31. J. Liu, G. Zhang, Z. Wang, Electrochemical behavior of Sn–xZn lead-free solders in aerated NaCl solution, in *2015 16th International Conference on Electronic Packaging Technology (ICEPT)*. (IEEE, Changsha, 2015), pp. 68–73
32. H. Huang, G. Shuai, X. Wei, C. Yin, Effects of sulfur addition on the wettability and corrosion resistance of Sn–0.7Cu lead-free solder. *Microelectron. Reliab.* **74**, 15–21 (2017)

33. C.W. See, M.Z. Yahaya, H. Haliman, A.A. Mohamad, Corrosion behavior of corroded Sn–3.0Ag–0.5Cu solder alloy. *Procedia Chem.* [Internet] **19**, 847–854 (2016). <https://doi.org/10.1016/j.proche.2016.03.112>
34. P. Marcus, V. Maurice, H.H. Strehblow, Localized corrosion (pitting): a model of passivity breakdown including the role of the oxide layer nanostructure. *Corros. Sci.* **50**(9), 2698–2704 (2008)
35. D.D. MacDonald, The history of the point defect model for the passive state: a brief review of film growth aspects. *Electrochim. Acta* [Internet] **56**(4), 1761–1772 (2011). <http://doi.org/10.1016/j.electacta.2010.11.005>
36. W.R. Osório, L.C. Peixoto, L.R. Garcia, A. Garcia, J.E. Spinelli, The effects of microstructure and Ag₃Sn and Cu₆Sn₅ intermetallics on the electrochemical behavior of Sn–Ag and Sn–Cu solder alloys. *Int. J. Electrochem. Sci* **7**, 6452 (2012)
37. W.R. Osório, E.S. Freitas, J.E. Spinelli, A. Garcia, Electrochemical behavior of a lead-free Sn–Cu solder alloy in NaCl solution. *Corros. Sci.* **80**, 71–81 (2014)
38. W.R. Osório, J.E. Spinelli, C.R.M. Afonso, L.C. Peixoto, A. Garcia, Microstructure, corrosion behaviour and microhardness of a directionally solidified Sn–Cu solder alloy. *Electrochim. Acta.* **56**(24), 8891–8899 (2011)
39. K. Kanlayasiri, K. Sukpimai, Effects of indium on the intermetallic layer between low-Ag SAC0307-xIn lead-free solders and Cu substrate. *J Alloys Compd.* **25**(668), 169–175 (2016)
40. J.C. Liu, S.W. Park, S. Nagao, M. Nogi, H. Koga, J.S. Ma et al., The role of Zn precipitates and Cl⁻ anions in pitting corrosion of Sn–Zn solder alloys. *Corros. Sci.* [Internet] **92**, 263–271 (2015). <https://doi.org/10.1016/j.corsci.2014.12.014>
41. Z. Wang, C. Chen, J. Liu, G. Zhang, K. Sukanuma, Corrosion mechanism of Zn–30Sn high-temperature, lead-free solder in neutral NaCl solution. *Corros. Sci.* [Internet] **140**, 40–50 (2018). <https://doi.org/10.1016/j.corsci.2018.06.025>
42. A. Aliyu, C. Srivastava, Correlation between growth texture, crystallite size, lattice strain and corrosion behavior of copper-carbon nanotube composite coatings. *Surf. Coatings Technol.* **405**, 126596 (2021)
43. A.V. Trukhanov, K.A. Darwish, M.M. Salem, O.M. Hemed, M.I. Abdel Ati, M.A. Darwish et al., Impact of the heat treatment conditions on crystal structure, morphology and magnetic properties evolution in BaM nanohexaferrites. *J. Alloys. Compd.* [Internet] **866**, 158961 (2021). <https://doi.org/10.1016/j.jallcom.2021.158961>

Publisher's Note Springer Nature remains neutral with regard to jurisdictional claims in published maps and institutional affiliations.